JOURNAL OF GEOPHYSICAL RESEARCH: ATMOSPHERES, VOL. 118, 965–976, doi:10.1029/2012JD018546, 2013

The ozone response to ENSO in Aura satellite measurements and a chemistry-climate simulation

Luke D. Oman,[1] Anne R. Douglass,[1] Jerry R. Ziemke,[1,2] Jose M. Rodriguez,[1] Darryn W. Waugh,[3] and J. Eric Nielsen[1,4]

Received 24 July 2012; revised 30 October 2012; accepted 7 December 2012; published 24 January 2013.

[1] The El Niño–Southern Oscillation (ENSO) is the dominant mode of inter-annual variability in the tropical ocean and troposphere. Its impact on tropospheric circulation causes significant changes to the distribution of ozone. Here we derive the lower tropospheric to lower stratospheric ozone response to ENSO from observations by the Tropospheric Emission Spectrometer (TES) and the Microwave Limb Sounder (MLS) instruments, both on the Aura satellite, and compare to the simulated response from the Goddard Earth Observing System Chemistry-Climate Model (GEOSCCM). Measurement ozone sensitivity is derived using multiple linear regression to include variations from ENSO as well as from the first two empirical orthogonal functions of the quasi-biennial oscillation. Both measurements and simulation show features such as the negative ozone sensitivity to ENSO over the tropospheric tropical Pacific and positive ozone sensitivity over Indonesia and the Indian Ocean region. Ozone sensitivity to ENSO is generally positive over the midlatitude lower stratosphere, with greater sensitivity in the Northern Hemisphere. GEOSCCM reproduces both the overall pattern and magnitude of the ozone response to ENSO obtained from observations. We demonstrate the combined use of ozone measurements from MLS and TES to quantify the lower atmospheric ozone response to ENSO and suggest its possible usefulness in evaluating chemistry-climate models.

Citation: Oman, L. D., A. R. Douglass, J. R. Ziemke, J. M. Rodriguez, D. W. Waugh, and J. E. Nielsen (2013), The ozone response to ENSO in Aura satellite measurements and a chemistry-climate simulation, *J. Geophys. Res.*, *118*, 965–976, doi:10.1029/2012JD018546.

1. Introduction

[2] Atmospheric and oceanic oscillations have a significant impact on the dynamics of the atmosphere. The El Niño–Southern Oscillation (ENSO) is a dominant driver of tropospheric variability on inter-annual timescales [*Philander*, 1989]. ENSO causes significant perturbations to both the oceanic and atmospheric circulations [*Bjerknes*, 1969; *Enfield*, 1989]. Changes in sea-surface temperature over the Pacific Ocean can change the location and intensity of convection, impacting both the Walker Circulation and inter-annual variability of the Hadley Cell [*Quan et al.*, 2004]. These changes in circulation impact the temperature and moisture fields over much of the tropical Pacific and have a significant impact on the chemical composition of the troposphere [*Chandra et al.*, 1998, 2002, 2009; *Peters et al.*, 2001; *Sudo and Takahashi*, 2001; *Ziemke and Chandra*, 2003; *Zeng and Pyle*, 2005; *Doherty et al.*, 2006; *Lee et al.*, 2010; *Randel and Thompson*, 2011]. ENSO has also been shown to influence stratospheric ozone distributions [*Randel and Cobb*, 1994; *Randel et al.*, 2009].

[3] The quasi-biennial oscillation (QBO) also contributes to inter-annual ozone variability in the tropical stratosphere [*Baldwin et al.*, 2001]. Several studies have suggested that the impact of the QBO can also be seen in tropospheric ozone [*Ziemke and Chandra*, 1999; *Chandra et al.*, 2002; *Lee et al.*, 2010; *Ziemke and Chandra*, 2012]. Circulation anomalies associated with the QBO have been found arching downward into the subtropical troposphere in a horseshoe-shaped pattern [*Crooks and Gray*, 2005; *Haigh et al.*, 2005].

[4] *Ziemke et al.* [2010] used data from several satellite instruments spanning over 30 years to investigate ENSO's impact on tropical tropospheric column ozone. The impact was so clear that they formed an Ozone ENSO Index (OEI) that was highly correlated to the Niño 3.4 Index. They calculated the OEI by subtracting the eastern and central tropical Pacific region tropospheric column ozone (15°S–15°N, 110°W–180°W) from the western tropical Pacific-Indian Ocean region (15°S–15°N, 70°E–140°E), and then removed the seasonal cycle and smoothed with a 3-month running average. *Oman et al.* [2011] used the Goddard Earth Observing System Chemistry-Climate Model (GEOSCCM) and found the OEI was reproduced in a 25-year simulation forced with observed sea-surface temperature variability. Also, they examined the vertical structure of the response

[1]NASA Goddard Space Flight Center, Greenbelt, Maryland, USA.
[2]Morgan State University, Baltimore, Maryland, USA.
[3]Johns Hopkins University, Baltimore, Maryland, USA.
[4]Science Systems and Applications Inc., Lanham, Maryland, USA.

Corresponding author: L. D. Oman, NASA Goddard Space Flight Center, Greenbelt, MA, USA. (luke.d.oman@nasa.gov)

2169-897X/13/2012JD018546

Table 1. Estimated Total Emissions Sources Used in the GEOSCCM Simulation

Source Category	NO_x, Tg N a^{-1}	CO, Tg C a^{-1}	VOC, Tg C a^{-1}
Fossil fuel	24.1	161.7	43.1
Biofuel	2.2	74.3	11.3
Biomass burning	5.3	180.6	13.8
Lightning	5.0		
Aircraft	0.6		

Volatile organic compounds (VOC) include C_4H_8O, C_3H6, C_2H_6, C_3H_8, C_4H_{10}, C_2H_4O, and CH_2O.

of ozone to ENSO and showed that the simulated response compared well with that derived from ozonesonde measurements at a few Southern Hemisphere Additional Ozonesondes (SHADOZ) locations. Here we compare the same model simulation to globally and vertically resolved ozone datasets from Aura satellite instruments. Previously, *Logan et al*. [2008] used Tropospheric Emission Spectrometer (TES) measurements and *Nassar et al*. [2009] used a chemical transport model to examine the chemical changes caused by the 2006 El Niño event and found significant increases in ozone, water vapor, and carbon monoxide (CO) over Indonesia and the Indian Ocean region.

[5] The Chemistry-Climate Model Validation (CCMVal) activity [*Eyring et al*., 2005; SPARC CCMVal, 2010] used process-oriented evaluation of models for understanding model performance and as a path for model improvement. The 2010 CCMVal report focused on stratospheric processes, and most of the evaluation criteria given in SPARC CCMVal [2010, Table 1.2] concern representation of some aspect of the mean state. *SPARC CCMVal* [2010, Table 1.2] is an overview of observations that were used to evaluate Chemistry-Climate models. Credibility in predictions made using CCMs is strengthened through evaluations that ensure their appropriate representation of large-scale atmospheric processes [*Strahan et al*., 2011]. It is important to demonstrate that a model responds to a natural forcing as observed and to understand that response. This provides a pathway toward understanding the response to an external perturbation. Building on the approach used in CCMVal, we look to extend this work in two ways, by participating in the next phase of CCMVal that will extend the domain that is evaluated to include the troposphere and also by focusing specifically on the fidelity of the model response to different forcings. Here we focus on the response of tropospheric ozone to ENSO as observed by satellite and test if the GEOSCCM successfully reproduces the observed response.

[6] The model, measurements, and methods used are described in the next section. The ozone response to ENSO as derived from measurements and our simulation are presented in section 3. In section 4, we discuss the method uncertainties and possible impacts of the QBO. Section 5 summarizes the main results and gives concluding remarks.

2. Model, Measurements, and Methods

[7] We examined the response of tropospheric and lower stratospheric ozone to ENSO in the Goddard Earth Observing System (GEOS) version 5 general circulation model [*Rienecker et al*., 2008] coupled to the comprehensive Global Modeling Initiative (GMI) stratosphere-troposphere chemical mechanism [*Duncan et al*., 2007; *Strahan et al*., 2007]. The GMI chemical mechanism includes 117 species, 322 chemical reactions, and 81 photolysis reactions. The SMVGEAR II algorithm [*Jacobson*, 1995] is used to integrate the chemical mass balance equations. The mechanism includes a detailed description of O_3-reactive Nitrogen oxides (NO_x)-hydrocarbon chemistry, which is described in *Duncan et al*. [2007]. The simulation has a horizontal resolution of 2° latitude by 2.5° longitude with 72 vertical layers up to 0.01 hPa (80 km). The simulation in this study was forced with observed sea-surface temperatures and sea ice concentrations from 1985 to 2009 [*Rayner et al*., 2003, updated on a monthly basis]. Other boundary conditions and emissions for trace gases are seasonally varying but annually repeating for 2005 conditions. Table 1 shows the annual emission for several important NO_x, CO, and volatile organic compounds (VOCs) sources used in the simulation. NO_x emitted by the soil and isoprene sources are calculated interactively in the model. *Lang et al*. [2012] compared the GEOSCCM tropospheric ozone concentrations to observations and found good agreement in the tropics and southern hemisphere, with a general high bias in the northern hemisphere middle to high latitudes.

[8] We used measurements from two instruments onboard the Aura satellite, the Tropospheric Emissions Spectrometer (TES) and the Microwave Limb Sounder (MLS). We used TES level 3 version 2 monthly mean measurements from September 2004 through December 2009 from 800 hPa to 261 hPa. TES measurements have been validated against ozonesonde profiles and have up to 2 degrees of freedom in the troposphere [*Nassar et al*., 2008]. TES has shown signs of aging, and beginning in January 2010, the frequency of TES observations decreased, limiting the ability to construct representative monthly means. Version 3.3 MLS level 2 profiles (from 261–56 hPa) were used to construct a monthly mean data set for August 2004 through May 2012 [*Livesey et al*., 2011]. Using the recommended quality and convergence threshold, the data were binned into 4° latitude by 5° longitude horizontal resolution. The MLS vertical resolution was retained. The MLS and TES data were treated separately in this analysis and were not merged at the 261 hPa interface.

[9] The ENSO index used in this study is based on the Niño 3.4 region and is available from the NOAA sea-surface temperature website (http://www.cpc.ncep.noaa.gov/data/indicies/). For the time period of the simulation (1985–2009), there are 12 ENSO events greater than ±1 standard deviation from the mean, 6 ENSO events over the 2004-2012 MLS observations, and 5 ENSO events over the 2004–2009 TES observations. A time series of monthly zonal winds from 70 to 10 hPa over Singapore (1°N, 104°E) is used to calculate the QBO empirical orthogonal functions (EOFs) [*Wallace et al*., 1993]. In this study, we use the first two EOFs which together account for just over 93% of the QBO variability. QBO EOF1 has a correlation of 0.97 with the 15 hPa minus 70 hPa observed zonal wind. QBO EOF2 has a correlation of 0.97 with 40 hPa observed zonal wind time series.

[10] We use either linear or multiple linear regression (MLR) analysis in this study to quantify the ozone response to a forcing. Linear regression is adequate to obtain the response of ozone to ENSO as simulated by GEOSCCM

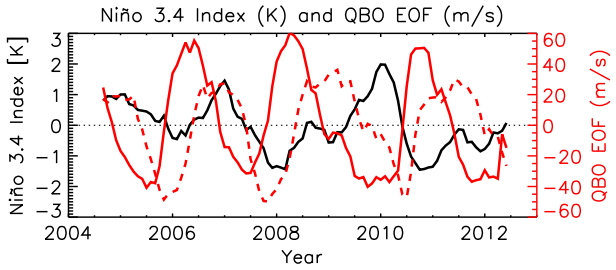

Figure 1. Time series of the Niño 3.4 Index (K) (solid black curve) and the first (solid red curve) and second (dashed red curve) empirical orthogonal functions of the QBO (m/s) from August 2004 to May 2012.

because the CCM does not simulate the QBO. Both the QBO and ENSO influence variability in the real atmosphere; therefore, MLR is used to derive ozone sensitivity to both forcings from MLS and TES observations. MLR has been used extensively in the stratosphere to separate causes of ozone trends [*Stolarski et al.*, 1991, 2006]. For example, the method has been used to quantify the ozone sensitivity to different mechanisms that may contribute to changes in upper stratospheric ozone in chemistry-climate simulations [*Oman et al.*, 2009, 2010]. For a given location and time, MLR is applied to determine the coefficients m_X such that

$$\Delta O_3(t) = \sum_j m_{X_j} \Delta X_j(t) + \varepsilon(t), \qquad (1)$$

where the X_j are the different quantities that could influence ozone (through different mechanisms) and the coefficients m_X are the sensitivity of ozone to the quantity X, that is, $m_X = \partial O_3/\partial X$. In the case of GEOSCCM, X_j is the Niño 3.4 Index from 1985 to 2009. For TES measurements, we use the Niño 3.4 Index, QBO EOF1, and QBO EOF2 for X_j from September 2004 to December 2009. We use the same three X_j for MLS except that the time series is from August 2004 to May 2012. Figure 1 shows the time series for Niño 3.4 Index (black curve), QBO EOF1 (solid red curve), and QBO EOF2 (dashed red curve). ENSO events have occurred with a periodicity similar to that of the QBO (~2.5 years) over this time period, causing correlations between ENSO and QBO EOFs. The correlation between Niño 3.4 Index and QBO EOF1 is −0.50 and between Niño 3.4 Index and QBO EOF2 is 0.19. The correlation between QBO EOF1 and QBO EOF2 is exactly zero by construction. Ideally, one would like to have completely independent forcings; however, this may not be possible with shorter duration observational data sets. Here we show that despite these correlations, the MLR reasonably separates these forcings.

3. Results

[11] *Oman et al.* [2011] showed that the sensitivity of tropospheric column ozone simulated with GEOSCCM to ENSO matched that obtained by analysis of a 25-year dataset for tropospheric column ozone. In addition, they compared simulated vertical ozone response with that obtained by analysis of a 12-year record of SHADOZ ozonesondes over two key tropical regions. The simulated response generally agreed with that derived from SHADOZ ozonesondes although there were some differences in the magnitude of the response. Here we extend the analyses to compare GEOSCCM to MLS/TES ozone observations from the lower troposphere to 20 km. The higher horizontal coverage of the MLS/TES measurements provides better spatial information than is available from SHADOZ, despite its lower vertical resolution and shorter record.

[12] Figure 2 shows an example of the MLR applied to MLS ozone measurements from 180°W to 110°W at 100 hPa over the equator. Figure 2a shows the deseasonalized ozone mixing ratio (black curve) and the regression fit (magenta curve) over the MLS time period with the mean MLS value of 102 ppb added to both curves. The regression analysis reasonably well reproduces the observed ozone changes over this region of the tropical Pacific Ocean. Figure 2b shows the individual contributions to the regression fit, with ENSO (red curve) and QBO EOF2 (green curve) generally showing larger contributions relative to QBO EOF1 (blue curve). The change over 2009 to 2010 stands out as the MLR suggest that a moderate/strong El Niño reduced ozone concentrations relative to smaller changes from the QBO. Differences at this location between measurements and the regression fit are largely due to higher frequency variability, which is not reproduced by the relatively lower frequency ENSO and QBO variability. Differences can especially be seen in the peak values during 2008 and 2011.

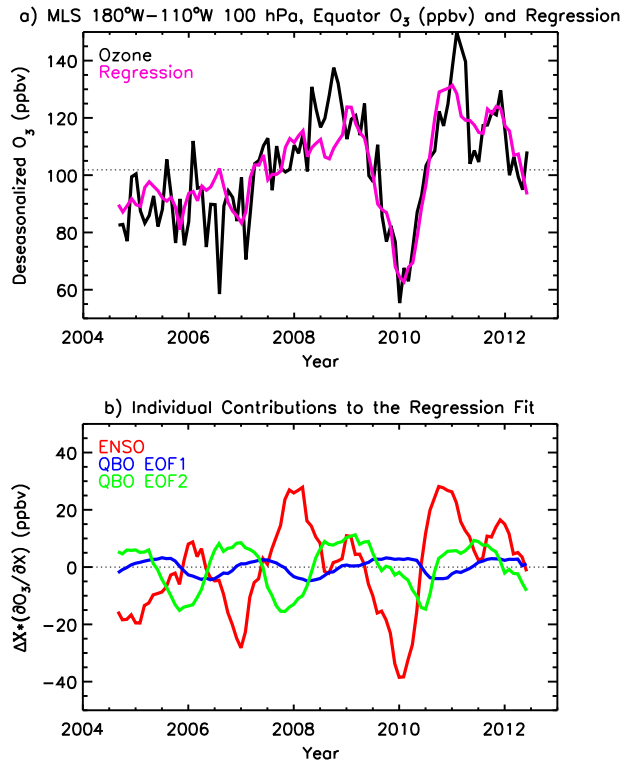

Figure 2. (a) The deseasonalized ozone concentrations from MLS averaged over 180°W–110°W, Equator at 100 hPa (black curve) and the regression fit (magenta curve) from August 2004 to May 2012. (b) The individual contributions to the regression fit from ENSO (red curve), QBO EOF1 (blue curve), and QBO EOF2 (green curve).

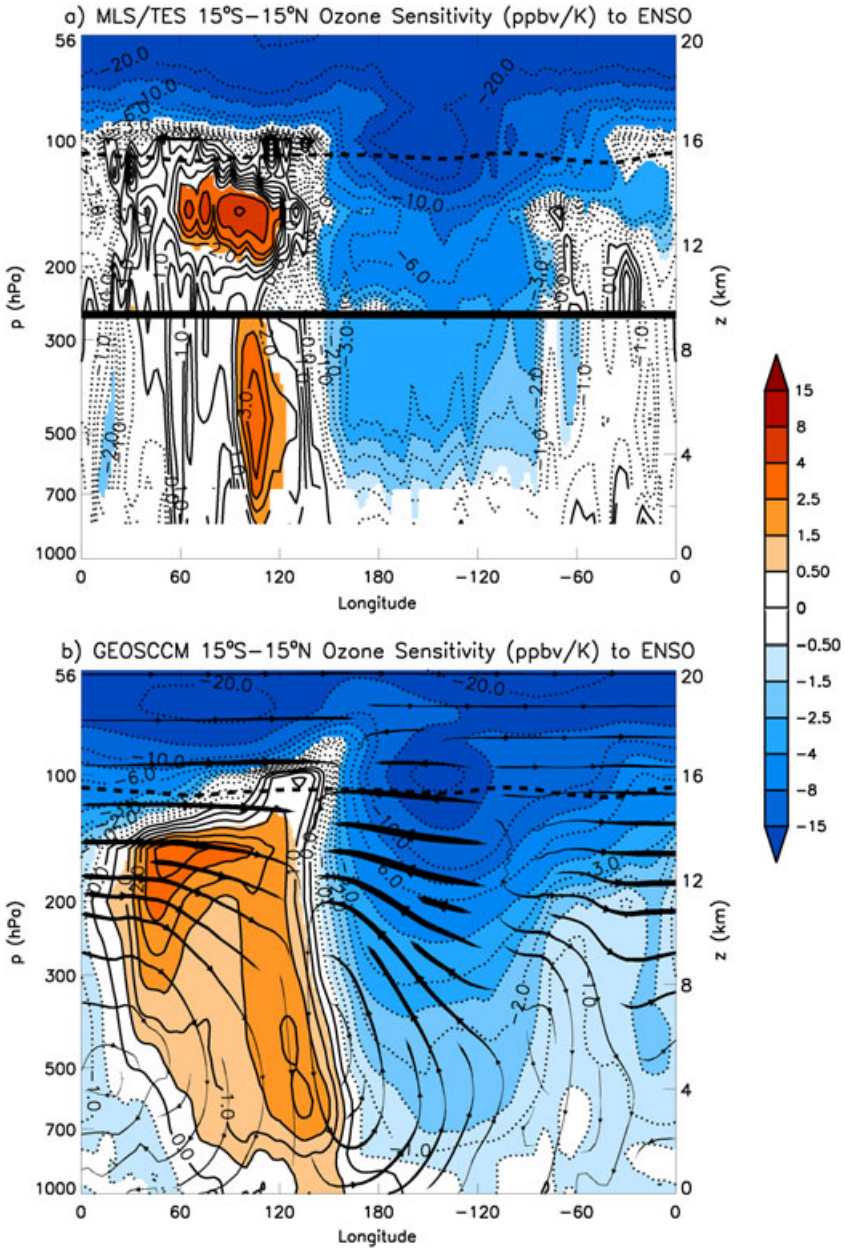

Figure 3. (a) MLS and TES sensitivity coefficients (ppbv/K) resulting from the Niño 3.4 Index component of the multiple linear regression using deseasonalized tropical (15°S–15°N) average ozone. (b) GEOSCCM sensitivity coefficients resulting from the linear regression of ozone against Niño 3.4 Index, over the same location. Overlaid is the anomalous circulation shown by the streamlines formed by regressing the zonal wind and vertical velocity against Nino 3.4 Index. Shaded regions are significant above 2 standard deviations, and the dashed black curve shows the mean model tropopause on both panels. The thick black line in Figure 3a at 261 hPa denotes the transition from TES measurements below and MLS above.

[13] We can now apply the MLR or linear regression to MLS/TES and GEOSCCM, respectively, over many locations and examine how the ozone sensitivity varies. We first focus on the tropical (15°S–15°N) response and then move to the eastern (180°W–110°W) and western (70°E–140°E) regions as defined by *Ziemke et al*. [2010] and used by *Oman et al*. [2011]. The measurement derived ozone sensitivity to ENSO is shown in Figure 3a obtained by multiple linearly regressing the deseasonalized tropical (15°S–15°N) average ozone at each longitude and pressure level against the Niño 3.4 Index and the first two EOFs of the QBO. A horizontal black line is drawn at 261 hPa to denote the transition from TES below to MLS above. ENSO-related ozone sensitivity coefficients show the linear response of ozone, in our case in parts per billion volume (ppbv), to a 1 K increase in the Niño 3.4 Index. In Figures 3–9, color

shading is done for areas significant above 2 standard deviations. The uncertainty estimates also include the impact of any autocorrelation in the residual term in the regression analysis [*Tiao et al.*, 1990]. Ozone sensitivity in the eastern region ranges from −1 to −3 ppbv/K in the lower troposphere to −10 to −20 ppbv/K near the tropopause. In the western region, the ozone sensitivity derived from measurements is positive with two local maxima, one in the mid-troposphere near 110°E of around 3 ppbv/K and a second in the upper troposphere closer to 4 ppbv/K. Negative ozone sensitivity is in the lower stratosphere at all longitudes.

[14] Figure 3b shows the ozone sensitivity coefficients from GEOSCCM obtained by linearly regressing the deseasonalized ozone over the same locations against the Niño 3.4 Index. The sensitivity derived from the GEOSCCM simulation exhibits a similar overall pattern to the MLS and TES measurements. In the troposphere, locations to the east of the International Date Line exhibit negative ozone sensitivity, while at locations to the west, ozone sensitivity to ENSO is positive. ENSO is known to cause significant changes in the tropical tropospheric circulation. The streamlines formed by regressing the zonal wind and vertical velocity against the Niño 3.4 Index overlies the ozone sensitivity in Figure 3b. The clear Walker circulation response lines up well with the pattern of ozone sensitivity. During an El Niño, there is an eastward shift in deep convection along with a consistent change in water vapor concentrations, both of which act to decrease ozone in the central and eastern Pacific Ocean. Negative sensitivity in the eastern region increases with height from 1–2 ppbv/K in the low to middle troposphere to 10–20 ppbv/K near the tropopause. The opposite impact occurs over the western region with decreased convection and water vapor. Figure 3b has two local maxima, one around 2 ppbv/K in the mid-troposphere near 130°E and a second in the upper troposphere around 3 ppbv/K. In the lower stratosphere, ozone generally decreases at all longitudes in the simulation, which is the same as seen in measurements.

[15] The GEOSCCM simulation has annually repeating biomass burning. To evaluate the impact of ENSO-related variations in biomass burning on ozone, we have analyzed a 10-year (1999–2008) simulation by the Global Modeling Initiative (GMI) chemical transport model [*Duncan et al.*, 2007; *Strahan et al.*, 2007] that includes inter-annual variations in biomass burning. This model is driven by meteorological fields from the Modern-Era Retrospective Analysis for Research and Applications (MERRA) reanalyses but has the same chemical mechanism. The GMI simulation indicates some differences over Indonesia and South America in the troposphere. In general, the simulation which includes biomass-burning and SST variability more closely matches the observed ozone sensitivity over Indonesia indicating that the smaller sensitivity in GEOSCCM is likely due to the lack of biomass-burning variability in the simulation. Significant differences are not seen over the eastern and central Pacific Ocean and in the lower stratosphere.

[16] We also examined the latitude dependence of ozone sensitivity and response of the circulation to ENSO. Figure 4a shows the MLS and TES ozone measurement sensitivity to ENSO over the eastern region (180°W–110°W). MLS measurements show negative sensitivity (6–20 ppbv/K) in the tropical upper troposphere that extends into the lower stratosphere. Over the midlatitudes, MLS shows positive ozone sensitivity between 261 and 80 hPa in the Southern Hemisphere and from 261 to at least 56 hPa in the Northern Hemisphere. There is excellent continuity between MLS- and TES-derived ozone sensitivity to ENSO in this region. The ozone sensitivity obtained from TES measurements is −2 to −3 ppbv/K in the deep tropics. TES ozone sensitivity is positive over the midlatitudes and extends to about 15°N in the mid-troposphere of the Northern Hemisphere. These regions of positive ozone sensitivity that extend into the troposphere mainly between 15° and 30° in each hemisphere could be consistent with increased stratosphere-troposphere exchange of ozone. *Zeng and Pyle* [2005] found increased stratosphere-troposphere exchange of ozone due to El Niño warming in a CCM simulation. More recently, *Voulgarakis et al.* [2011] also found increased stratosphere-troposphere exchange of ozone from the 1997–1998 El Niño in a chemical transport model. Observation taken over Colorado by *Langford et al.* [1998] and *Langford* [1999] also showed evidence of increased ozone in the troposphere during El Niño.

[17] Figure 4b shows the ozone sensitivity to ENSO over the same region from GEOSCCM. We see overall excellent pattern agreement between this model simulation and observations; however, there are differences between 56 and 100 hPa over the midlatitude SH where the MLS ENSO ozone sensitivity is mostly not significant. The change in circulation is shown by the streamlines formed from regressing the meridional wind and vertical velocity against the Niño 3.4 Index. The GEOSCCM shows a stronger mean ascending branch of the Walker circulation near the equator for an El Niño warming which is collocated with negative ozone sensitivity ranging from 2–3 ppbv/K in the low to middle troposphere to 10–15 ppbv/K near the tropopause. In the subtropical upper troposphere, the decreased ozone sensitivity is collocated with meridional flow out of the deep tropics. The measurements show a similar pattern to that obtained from GEOSCCM in the tropical troposphere although broader in latitude. There is remarkably good agreement between measurements and the simulation in the tropical upper troposphere, which extends into the tropical lower stratosphere. The GMI simulation including biomass-burning variability shows similar ozone variability over this region compared to GEOSCCM. This indicates that inter-annual variability in biomass burning does not play a major role in ozone variability in this region.

[18] The tropospheric ozone response in the western region (70°E–140°E), shown in Figure 5, differs substantially from that in the eastern region. Figure 5 shows the ozone sensitivity derived from (a) MLS and TES measurements and (b) GEOSCCM. Both the measurements and the model show a positive ozone response in the tropical troposphere and a negative ozone response in the tropical stratosphere like that seen in the eastern region. The simulation shows anomalous downwelling over the deep tropical troposphere, again consistent with observed circulation response to ENSO [*Quan et al.*, 2004] and associated positive ozone sensitivity throughout the deep tropical troposphere. There are three local maxima, one in the mid-troposphere from 10°S-Eq. and the other two in the upper troposphere, near the equator and 20°S. Ozone sensitivity in the extratropical troposphere is generally negative. The lower stratospheric response is more asymmetric than that seen in the eastern region, where

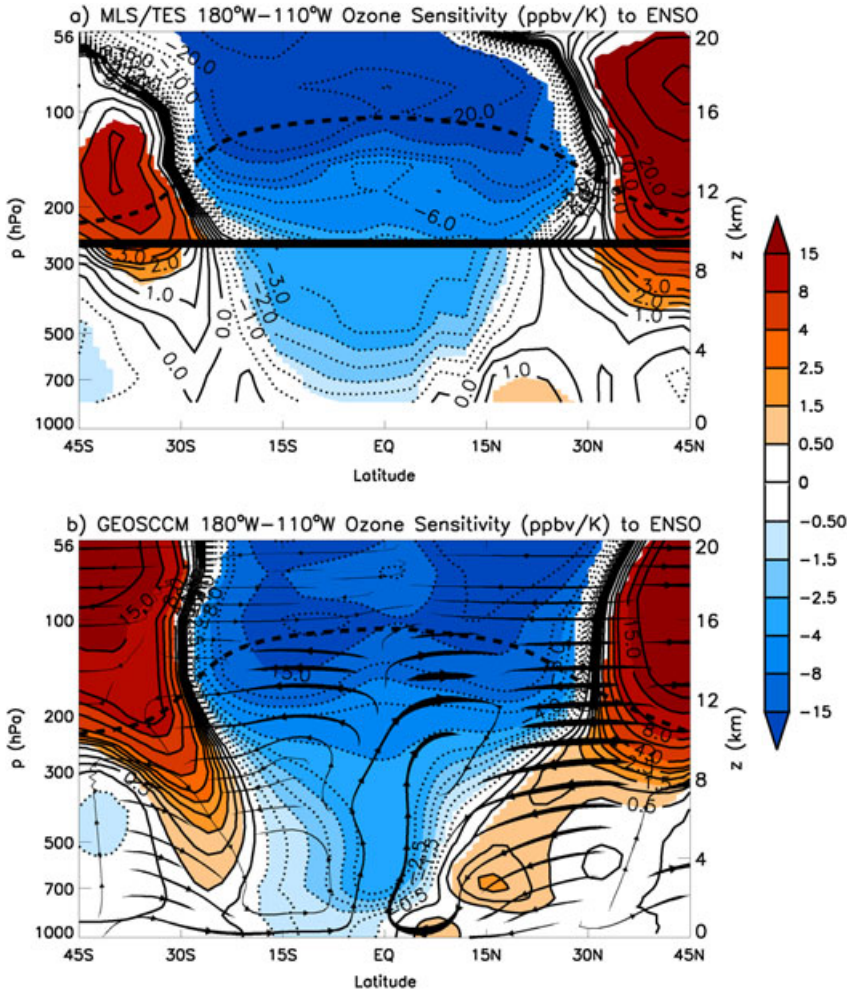

Figure 4. (a) MLS and TES sensitivity coefficients (ppbv/K) resulting from the Niño 3.4 Index component of the multiple linear regression using deseasonalized eastern region (180°W–110°W) average ozone. (b) GEOSCCM sensitivity coefficients resulting from the linear regressing of ozone against Niño 3.4 Index, over the same location. Overlaid is the anomalous circulation shown by the streamlines formed by regressing the meridional wind and vertical velocity against Niño 3.4 Index. Shaded regions are significant above 2 standard deviations, and the dashed black curve shows the mean model tropopause on both panels.

ozone sensitivity in the Northern Hemisphere midlatitudes is positive between 30° and 45°.

[19] *Chandra et al.* [1998] suggested that downward motion, suppressed convection, and a drier troposphere all contributed to the increase in ozone seen over the tropical western Pacific and Indonesian region. The combination of downward motion and suppressed convection allows higher ozone concentrations from the upper troposphere to be transported downward [*Sudo and Takahashi*, 2001] and reduces the upward transport of low ozone air over ocean surfaces. The drier troposphere also increases the chemical lifetime of ozone, which causes increased tropospheric ozone concentrations [*Kley et al.*, 1996]. The ozone changes seen in Figure 5 in both simulation and measurements are consistent in sign with those expected from these previous studies. Over the extratropical troposphere, the ozone sensitivity derived from observations is negative in the Southern Hemisphere. The sensitivity derived from observations is asymmetric in the midlatitude lower stratosphere and similar to that derived from GEOSCCM, with negative sensitivity in the Southern Hemisphere and positive in the Northern Hemisphere. The GMI simulation including biomass-burning variability does show a larger ozone response in the tropical troposphere than GEOSCCM and typically is in closer agreement with MLS/TES observations. This indicates that inter-annual variability in biomass burning does contribute to ozone variability in this region.

[20] We also examined the 150 hPa level globally to compare variations in the pattern of horizontal ozone sensitivity. Figure 6a shows the ozone sensitivity derived from MLS measurements at 147 hPa using MLR. Over the tropical Pacific and Atlantic Oceans, negative ozone sensitivity dominates with dual local minima over the central Pacific of −15 ppbv/K approximately 15–20° off the equator in each hemisphere. These anomalies are strongly influenced by the increased horizontal poleward flow as shown in Figure 4b. Positive ozone sensitivity is seen over much of the tropical Indian Ocean and in bands across much of the midlatitudes

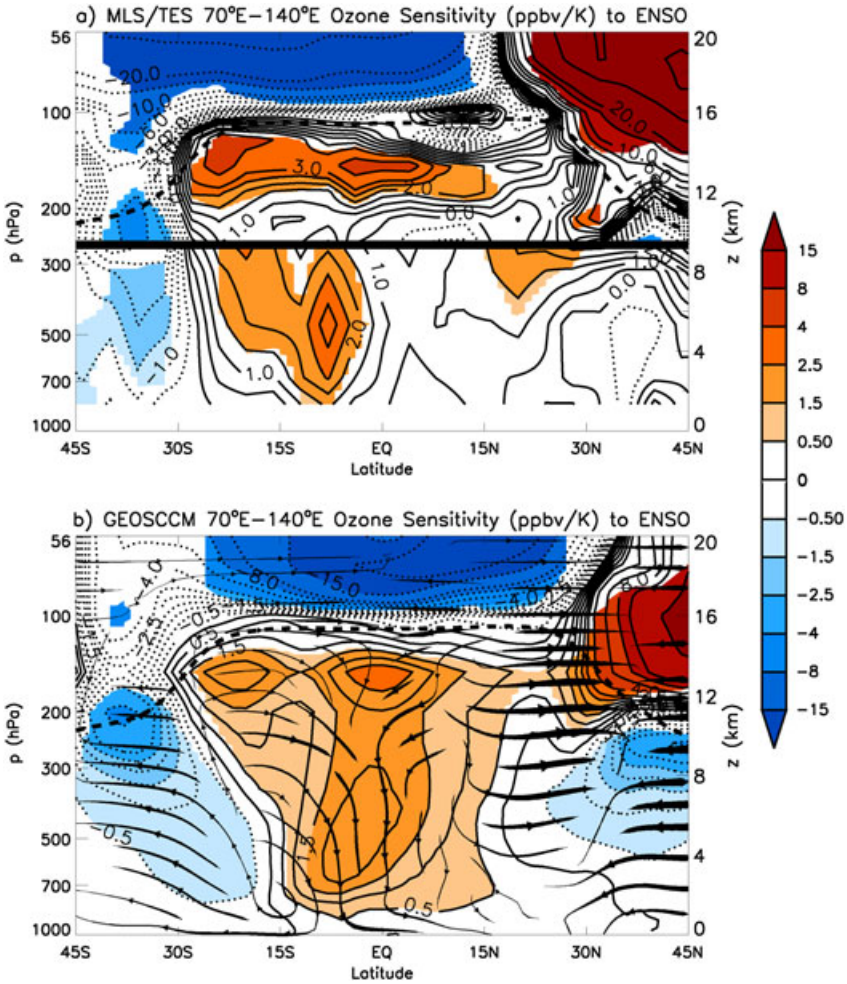

Figure 5. (a) MLS and TES sensitivity coefficients (ppbv/K) resulting from the Niño 3.4 Index component of the multiple linear regression using deseasonalized western region (70°E–140°E) average ozone. (b) GEOSCCM sensitivity coefficients resulting from the linear regressing of ozone against Niño 3.4 Index, over the same location. Overlaid is the anomalous circulation shown by the streamlines formed by regressing the meridional wind and vertical velocity against Niño 3.4 Index. Shaded regions are significant above 2 standard deviations, and the dashed black curve shows the mean model tropopause on both panels.

of both hemispheres. Figure 6b shows the GEOSCCM ozone sensitivity at 150 hPa obtained by linearly regressing the deseasonalized ozone at each latitude and longitude against the Niño 3.4 Index. The pattern from the GEOSCCM simulation is very similar to that obtained from MLS measurements. The ozone sensitivity is negative (−15 ppbv/K) in a large region between 30°S–30°N and east of 140°E, peaking over the central Pacific Ocean similarly to the MLS measurements. Ozone sensitivity is positive over Indonesia and much of the tropical Indian Ocean. Also, bands of positive ozone sensitivity occur at midlatitudes of both hemispheres with local maxima over the Pacific Ocean and greater sensitivity in the Northern Hemisphere.

4. QBO Sensitivity and Uncertainties

[21] In addition to ENSO, the QBO has been shown to influence ozone in the stratosphere [*Randel and Cobb*, 1994] and to a lesser extent in the troposphere [*Ziemke and Chandra*, 1999; *Lee et al.*, 2010; *Ziemke and Chandra*, 2012]. Since ENSO and the QBO impact ozone, it is necessary to include both in the regression analysis. In this section, we show the impact of the first two EOFs of the QBO on ozone and discuss areas where there is likely not complete separation of the ENSO and QBO signals. GEOSCCM used in the present work does not simulate the QBO, so we only consider results from the MLR of MLS and TES measurements.

[22] First we examine the tropical 15°S–15°N average ozone sensitivity to the two EOFs, similar to that shown for ENSO in Figure 3a. Figure 7 shows the MLS and TES ozone sensitivity (ppbv/20 m s^{-1}) for the first (Figure 7a) and second (Figure 7b) EOFs of the QBO. As expected, the ozone sensitivity is largest in the stratosphere, and there are no large ENSO-like features. Smaller features (on order 0.5 ppbv/20 m s^{-1}) in the TES QBO EOF1 do appear

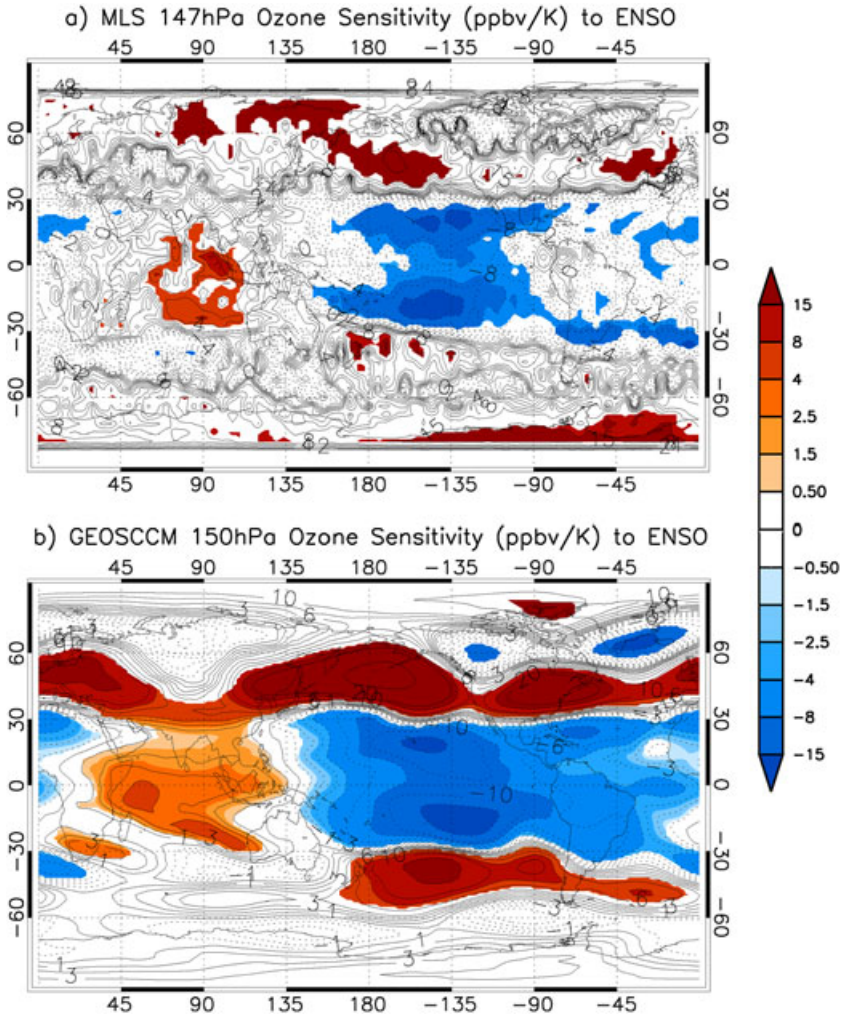

Figure 6. (a) MLS sensitivity coefficients (ppbv/K) at 147 hPa, resulting from the Niño 3.4 Index component of the multiple linear regression. (b) GEOSCCM sensitivity coefficients resulting from linearly regressing deseasonalized 150 hPa average ozone against Niño 3.4 Index. Shaded regions are significant above 2 standard deviations in both panels.

ENSO-like. Due to the negative correlations between ENSO and QBO, EOF1 would act to slightly reduce the ENSO derived sensitivity over those regions. *Ziemke and Chandra* [2012] found a persistent negative correlation between the QBO, as measured at 50 hPa over Singapore, and 32-year observed tropical Atlantic (60°W–60°E, 5°S–5°N) tropospheric column ozone record. The magnitude of the response varied over time but typically averaged around 4 DU over a QBO cycle and closer to 2 DU during the Aura satellite period.

[23] Figure 8 shows the eastern region (180°W–110°W) QBO EOF ozone sensitivity. In the deep tropical lower stratosphere, ozone sensitivity to EOF1 is negative, with larger positive sensitivity to EOF2 especially near 56 hPa. Also, sensitivity to EOF2 extends into the upper tropical troposphere with values up to 4 ppbv/20 m s^{-1} near the tropopause. *Crooks and Gray* [2005] found a significant horseshoe-like pattern in the tropospheric zonal wind response to the second principle component of the QBO (similar to our QBO EOF2) in the ERA-40 reanalysis. Figure 8b shows that this feature is consistent with the ozone response seen in MLS with two lobes extending into the subtropical lower stratosphere. The derived ozone sensitivities from QBO EOF2 have a bigger impact in the tropics below 56 hPa than that from QBO EOF1, which is consistent with the temperature and circulation features shown in *Crooks and Gray* [2005]. Significant negative ozone sensitivities extend into the NH midlatitude troposphere from the QBO EOF2 seen in Figure 8b, which is consistent with significant zonal wind changes found by *Crooks and Gray* [2005] in ERA-40 reanalysis.

[24] The ozone sensitivity to the QBO EOFs in the western region (70°E–140°E) is shown in Figure 9. Since the stratospheric QBO forcing is fairly symmetric, both regions exhibit similar lower stratospheric response in the tropics and midlatitudes. Relatively small ENSO-like features in the EOF1 are apparent in the troposphere, for example, the region of small positive ozone sensitivity in the tropical Southern Hemisphere. The upper troposphere ozone sensitivity to QBO EOF2 is positive, similar to the eastern region.

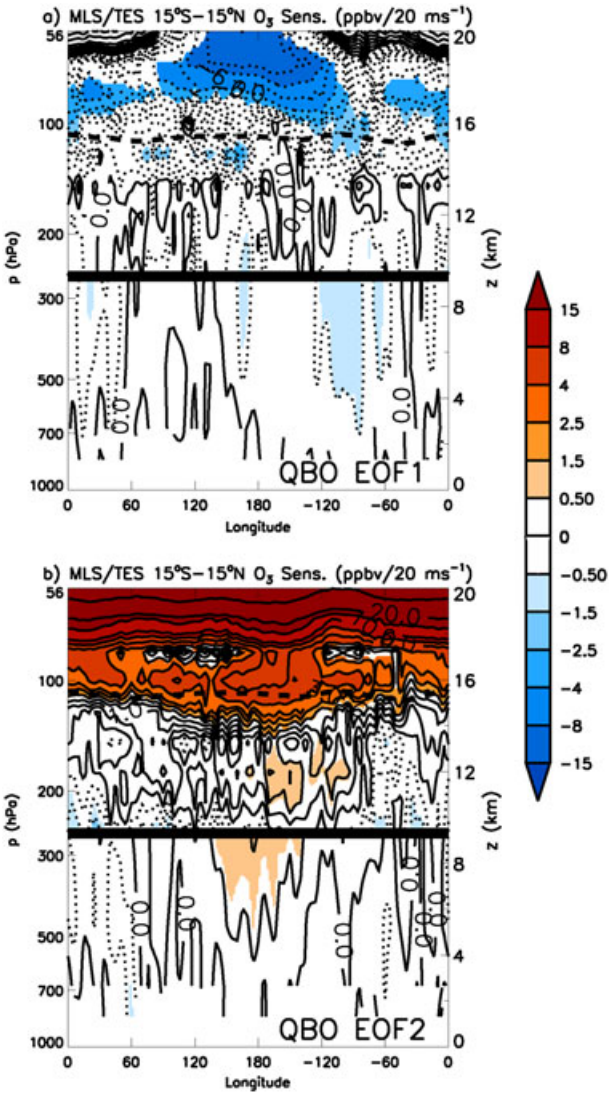

Figure 7. MLS and TES sensitivity coefficients (ppbv/20 m s^{-1}) from the multiple linear regression analysis using deseasonalized tropical (15°S–15°N) average ozone for the first (a) and second (b) EOF of the QBO. Shaded regions are significant above 2 standard deviations in both panels.

Lee et al. [2010] discussed finding ozone anomalies due to the QBO in SHADOZ measurements of up to 8 ppbv in the upper troposphere. This size anomaly is consistent with the QBO EOF2 ozone sensitivity of 4 ppbv/20 m s^{-1} found here using MLS measurements since the EOF2 typically varies between ±40 m/s (shown in Figure 1) over a typical QBO cycle.

[25] As mentioned in section 2, the negative correlation between ENSO and QBO EOF1 makes complete separation of the forcings using MLR not possible. Extending the observational record would improve the separation of atmospheric processes if the correlation decreased with additional years. Unfortunately, TES did not make sufficient measurements to produce meaningful monthly mean fields after January 2010. Additionally, the use of multiple linear regression would not allow the representation of any nonlinear ozone responses. *Hoerling et al*. [1997] showed that differences in the teleconnections do occur between El Nino and La Nina most notably in the midlatitudes.

[26] Other factors such as the strength of the Brewer-Dobson circulation also play a role in the ozone concentrations in the UT/LS [*Randel et al*., 2007]. If these circulation changes are due to ENSO [*Calvo et al*., 2010] or the QBO [*Baldwin et al*., 2001], they should be represented in this regression analysis; however, other factors not considered here could also impact the strength of this circulation. Solar cycle variations could also impact lower atmospheric ozone [*Chandra et al*., 1999]; however, due to the relative shortness of the observational record compared to the length of a solar cycle, it is not included in this analysis. MLR tests which include a measure of solar cycle variability did not appear to significantly

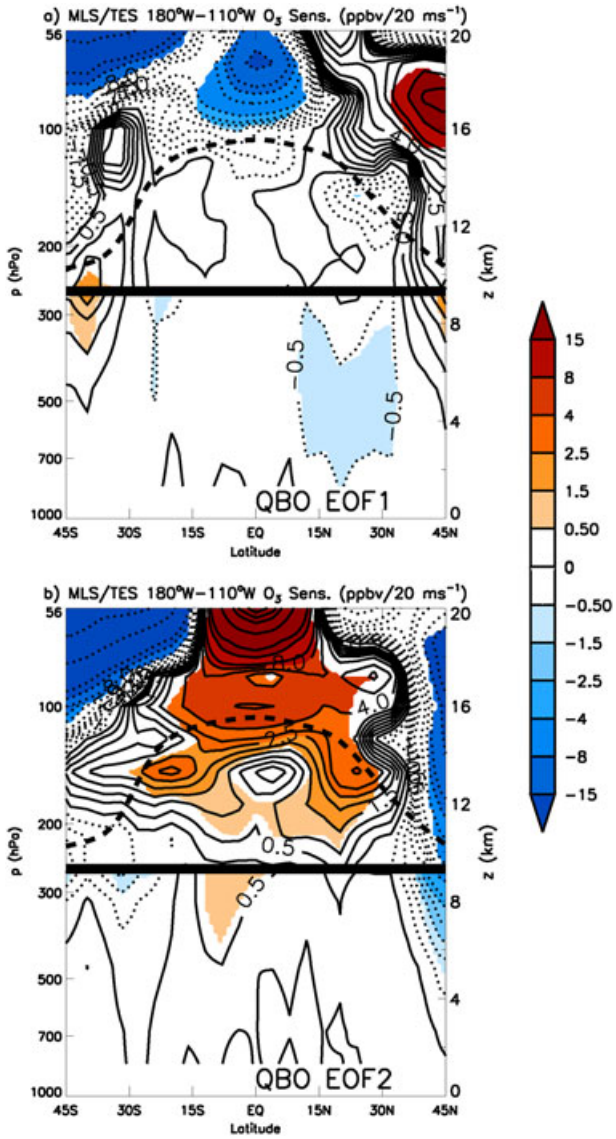

Figure 8. MLS and TES sensitivity coefficients (ppbv/20 m s^{-1}) from the multiple linear regression analysis using deseasonalized eastern region (180°W–110°W) average ozone for the first (a) and second (b) EOF of the QBO. Shaded regions are significant above 2 standard deviations in both panels.

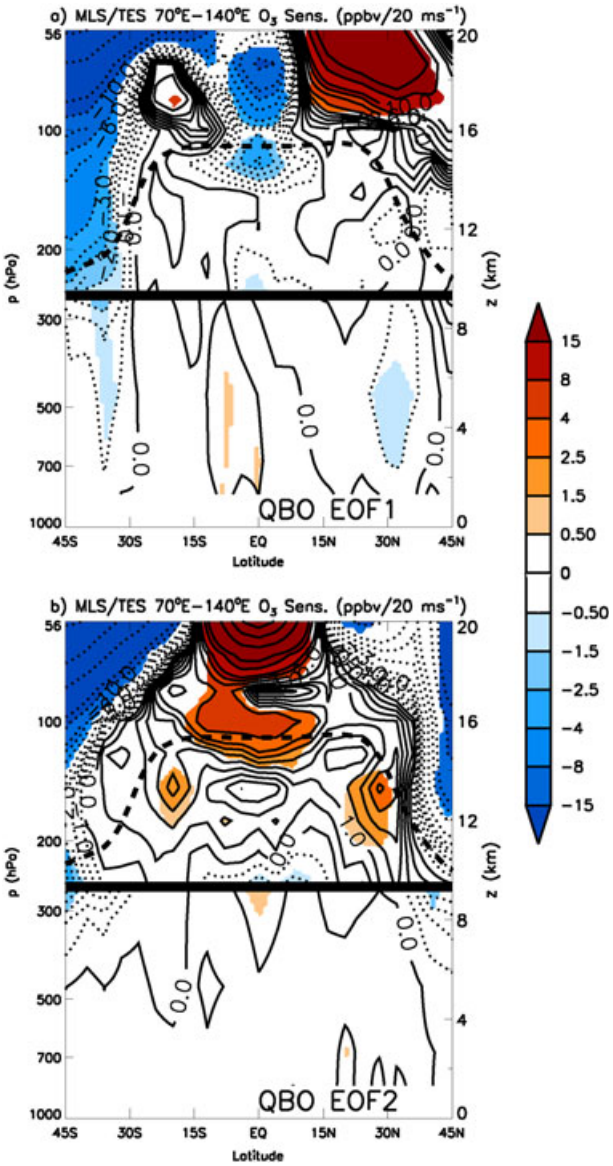

Figure 9. MLS and TES sensitivity coefficients (ppbv/20 m s^{-1}) from the multiple linear regression analysis using deseasonalized western region (70°E–140°E) average ozone for the first (a) and second (b) EOF of the QBO. Shaded regions are significant above 2 standard deviations in both panels.

impact the derived ENSO and QBO ozone sensitivities. Also, excluding the QBO from the regression analysis does not significantly change the ENSO derived ozone response but does increase the uncertainty since the autocorrelation is increased in the residual term.

5. Discussion and Conclusions

[27] This study presents observations of the response of ozone to ENSO from the lower troposphere to the lower stratosphere and compares the response derived from observations with that obtained from a GEOSCCM simulation. We use a combination of MLS and TES measurements from the Aura satellite platform to derive the ozone response from the troposphere to the lower stratosphere. ENSO variations are a dominant driver of tropical Pacific upper tropospheric ozone variability.

[28] The tropical tropospheric ozone sensitivity to ENSO is negative over much of Pacific and Atlantic Oceans and positive over Indonesia and the Indian Ocean. This result is seen in MLS and TES measurements and reproduced by the GEOSCCM forced with observed sea-surface temperatures. Ozone sensitivity to ENSO is negative in the tropical lower stratosphere over all longitudes.

[29] The eastern regional (180°W–110°W) ozone sensitivity from both simulation and measurements is negative in the tropics and is larger in the upper troposphere and lower stratosphere. Ozone sensitivity is positive over the midlatitudes in the upper troposphere and lower stratosphere in measurements and simulations. There is excellent continuity in the ozone response to ENSO derived from MLS and TES measurements near 261 hPa.

[30] The western regional (70°E–140°E) response with positive ozone sensitivity over the tropical troposphere is seen in GEOSCCM and measurements as well as negative sensitivity in the tropical lower stratosphere. In the lower stratosphere midlatitudes, an asymmetric response is produced in simulation and measurements, where negative ozone sensitivity occurs in the Southern Hemisphere and positive ones in the Northern Hemisphere.

[31] GEOSCCM reproduces the horizontal pattern and response magnitude at around 150 hPa as derived from MLS measurements. The results presented here showing a tropical upper tropospheric QBO-induced ozone change in MLS measurements are consistent with the findings of *Lee et al.* [2010] using the SHADOZ ozonesonde record.

[32] This work shows a clear ozone response to ENSO that is observed in MLS/TES measurements and can be reproduced in a GEOSCCM simulation; however, some differences are seen. A GMI simulation that includes biomass-burning variability does reduce some of the differences between GEOSCCM and observations, especially over Indonesia. Some differences are also seen over South America but are not significant in the observed ozone sensitivity to ENSO. Examining the response from atmospheric processes such as ENSO represents an excellent test for CCMs. It requires the proper simulation of horizontal and vertical gradients of ozone in the lower atmosphere along with the appropriate dynamical representation of a large-scale atmospheric process like ENSO. Tests such as these could provide a useful tool in the evaluation of CCMs. Continued work needs to be done to determine if the response of tropospheric ozone to ENSO is useful for understanding prediction of ozone evolution. Changes in the frequency, magnitude, or type of ENSO could impact tropospheric composition. Such changes in ENSO could result from climate change or could be important on decadal time scales through the Pacific Decadal Oscillation.

[33] **Acknowledgments.** This research was supported by the NASA MAP, ACMAP, and Aura programs. We would like to thank Stacey Frith for helping with the model output processing, Jacquie Witte and Mike Manyin for the help with the measurement data sets, Feng Li for the comments on an early version of this manuscript, and the three

anonymous reviewers for their very helpful comments. We also thank those involved in model development at GSFC and the high-performance computing resources that were provided by NASA's Advanced Supercomputing Division.

References

Baldwin, M. P., et al. (2001), The quasi-biennial oscillation, *Rev. Geophys.*, *39*(2), 179–229, doi:10.1029/1999RG000073.

Bjerknes, J. (1969), Atmospheric teleconnections from the equatorial Pacific, *Mon. Weather Rev.*, *18*, 820–829.

Calvo, N., R. R. Garcia, W. J. Randel, and D. Marsh (2010), Dynamical mechanism for the increase in tropical upwelling in the lowermost tropical stratosphere during warm ENSO events, *J. Atmos. Sci.*, *67*, 2331–2340.

Chandra, S., J. R. Ziemke, W. Min, and W. G. Read (1998), Effects of 1997–1998 El Niño on tropospheric ozone and water vapor, *Geophys. Res. Lett.*, *25*, 3867–3870.

Chandra, S., J. R. Ziemke, and R. W. Stewart (1999), An 11-year solar cycle in tropospheric ozone from TOMS measurements, *Geophys. Res. Lett.*, *26*(2), 185–188, doi:10.1029/1998GL900272.

Chandra, S., J. R. Ziemke, P. K. Bhartia, and R. V. Martin (2002), Tropical tropospheric ozone: Implications for dynamics and biomass burning, *J. Geophys. Res.*, *107*(D14), 4188, doi:10.1029/2001JD000447.

Chandra, S. J. R. Ziemke, B. N. Duncan, T. L. Diehl, N. J. Livesey, and L. Froidevaux (2009), Effects of the 2006 El Niño on tropospheric ozone and carbon monoxide: Implications for dynamics and biomass burning, *Atmos. Chem. Phys.*, *9*, 4239–4249.

Crooks, S. A., and L. J. Gray (2005), Characterization of the 11-year solar signal using a multiple regression analysis of the ERA-40 dataset, *J. Clim.*, *18*, 996–1015.

Doherty, R. M., D. S. Stevenson, C. E. Johnson, W. J. Collins, and M. G. Sanderson (2006), Tropospheric ozone and El Niño–Southern Oscillation: Influence of atmospheric dynamics, biomass burning emissions, and future climate change, *J. Geophys. Res.*, *111*, D19304, doi:10.1029/2005JD006849.

Duncan, B. N., S. E. Strahan, Y. Yoshida, S. D. Steenrod, and N. Livesey, (2007), Model study of the cross-tropopause transport of biomass burning pollution, *Atmos. Chem. Phys.*, *7*, 3713–3736.

Enfield, D. B. (1989), El Niño, past and present, *Rev. Geophys.*, *27*(1), 159–187, doi:10.1029/RG027i001p00159.

Eyring, V., et al. (2005), A strategy for process-oriented validation of coupled chemistry-climate models, *Bull. Am. Meteorol. Soc.*, *86*, 1117–1133.

Haigh, J. D., M. Blackburn, and R. Day (2005), The response of tropospheric circulation to perturbations in lower-stratospheric temperature. *J. Clim.*, *18*, 3672–3685.

Hoerling, M. P., A. Kumar, and M. Zhong (1997), El Niño, La Niña, and the nonlinearity of their teleconnections, *J. Clim.*, *10*, 1769–1786.

Jacobson, M. Z. (1995), Computation of global photochemistry with SMVGEAR II, *Atmos. Environ.*, *29*, 2541–2546.

Kley, D., P. J. Crutzen, H. G. J. Smit, H. Vomel, S. J. Oltmans, H. Grassl, and V. Ramanathan (1996), Observations of near-zero ozone concentrations over the convective Pacific: Effects on air chemistry, *Science*, *274*, 230–233.

Lang, C., D. W. Waugh, M. A. Olsen, A. R. Douglass, Q. Liang, J. E. Nielsen, L. D. Oman, S. Pawson, and R. S. Stolarski (2012), The impact of greenhouse gases on past changes in tropospheric ozone, *J. Geophys. Res.*, *117*, D23304, doi:10.1029/2012JD018293.

Langford, A. O., T. J. O'Leary, C. D. Masters, K. C. Aikin, and M. H. Proffitt (1998), Modulation of middle and upper tropospheric ozone at Northern midlatitudes by the El Niño/Southern Oscillation, *Geophys. Res. Lett.*, *25*, 2667–2670.

Langford, A. O. (1999), Stratosphere-troposphere exchange at the subtropical jet: contribution to the tropospheric ozone budget at midlatitudes, *Geophys. Res. Lett.*, *26*, 2449–2452.

Lee, S., D. M. Shelow, A. M. Thompson, and S. K. Miller (2010), QBO and ENSO variability in temperature and ozone from SHADOZ, 1998–2005, *J. Geophys. Res.*, *115*, D18105, doi:10.1029/2009JD013320.

Livesey, N. J., et al. (2011), Earth Observing System (EOS) Aura Microwave Limb Sounder (MLS) version 3.3 level 2 data quality and description document, JPL D-33509, Jet Propulsion Laboratory, California Institute of Technology, Pasadena, California, USA, 162 pp.

Logan, J. A., I. Megretskaia, R. Nassar, L. T. Murray, L. Zhang, K. W. Bowman, H. M. Worden, and M. Luo (2008), Effects of the 2006 El Nino on tropospheric composition as revealed by data from the Tropospheric Emission Spectrometer (TES), *Geophys. Res. Lett.*, *35*, L03816, doi:10.1029/2007GL031698.

Nassar, R., et al. (2008), Validation of Tropospheric Emission Spectrometer (TES) nadir ozone profiles using ozonesonde measurements, *J. Geophys. Res.*, *113*, D15S17, doi:10.1029/2007JD008819.

Nassar, R., J. A. Logan, I. A. Megretshaia, L. T. Murray, L. Zhang, and D. B. A. Jones (2009), Analysis of tropical tropospheric ozone, carbon monoxide, and water vapor during the 2006 El Nino using TES observations and the GEOS-Chem model, *J. Geophys. Res.*, *114*, D17304, doi:10.1029/2009JD011760.

Oman, L., D. W. Waugh, S. R. Kawa, R. S. Stolarski, A. R. Douglass, and P. A. Newman (2009), Mechanisms and feedbacks causing changes in upper stratospheric ozone in the 21st century, *J. Geophys. Res.*, *114*, doi:10.1029/2009JD012397.

Oman, L. D., et al. (2010), Multimodel assessment of the factors driving stratospheric ozone evolution over the 21st century, *J. Geophys. Res.*, *115*, D24306, doi:10.1029/2010JD014362.

Oman, L. D., J. R. Ziemke, A. R. Douglass, D. W. Waugh, C. Lang, J. M. Rodriguez, J. E. Nielsen (2011), The response of tropical tropospheric ozone to ENSO, *Geophys. Res. Lett.*, *38*, doi:10.1029/2011GL047865.

Peters, W., M. Krol, F. Dentener, and J. Lelieveld (2001), Identification of an El Nino Southern Oscillation signal in a multiyear global simulation of tropospheric ozone. *J. Geophys. Res.*, *106*, 10,389–10,402.

Philander, S. G. (1989), El Niño, La Nina, and the Southern Oscillation, pp. 293, Academic Press, San Diego, California, United States.

Quan, X.-W., H. F. Diaz, and M. P. Hoerling (2004), Change in the tropical Hadley cell since 1950, in *The Hadley Circulation: Past, Present, and Future*, edited by H. F. Diaz and R. S. Bradley, Cambridge Univ. Press, New York.

Randel, W. J., and J. B. Cobb (1994), Coherent variations of monthly mean total ozone and lower stratospheric temperature. *J. Geophys. Res.*, *99*, 5433–5477.

Randel, W. J., M. Park, F. Wu, and N. Livesey (2007), A large annual cycle in ozone above the tropical tropopause linked to the Brewer-Dobson circulation, *J. Atmos. Sci.*, *64*, 4479–4488.

Randel, W. J., R. R. Garcia, N. Calvo, and D. Marsh (2009), ENSO influence on zonal mean temperature and ozone in the tropical lower stratosphere, *Geophys. Res. Lett.*, *36*, L15822, doi:10.1029/2009GL039343.

Randel, W. J., and A. M. Thompson (2011), Interannual variability and trends in tropical ozone derived from SAGE II satellite data and SHADOZ ozonesondes, *J. Geophys. Res.*, *116*, D07303, doi:10.1029/2010JD015195.

Rayner, N. A., D. E. Parker, E. B. Horton, C. K. Folland, L. V. Alexander, D. P. Rowell, E. C. Kent, and A. Kaplan (2003), Global analyses of sea surface temperature, sea ice, and night marine air temperature since the late nineteenth century, *J. Geophys. Res.*, *108*(D14), 4407, doi:10.1029/2002JD002670.

Rienecker, M. M., et al. (2008), The GEOS-5 data assimilation system—Documentation of versions 5.0.1, 5.1.0, and 5.2.0. *Technical Report Series on Global Modeling and Data Assimilation*, 27.

SPARC CCMVal (2010), *SPARC Report on the Evaluation of Chemistry-Climate Models*, V. Eyring, T. G. Shepherd, D. W. Waugh (Eds.), SPARC Report No. 5, WCRP-132, WMO/TD-No. 1526, http://www.atmosp.physics.utoronto.ca/SPARC.

Stolarski, R. S., P. Bloomfield, R. D. McPeters, and J. R. Herman (1991), Total ozone trends deduced from *Nimbus-7* TOMS data, *Geophys. Res. Lett.*, *18*, 1015–1018.

Stolarski, R. S., A. R. Douglass, S. Steenrod, and S. Pawson (2006), Trends in stratospheric ozone: Lessons learned from a 3D chemical transport model, *J. Atmos. Sci.*, *63*, 1028–1041.

Strahan, S. E., B. N. Duncan and P. Hoor (2007), Observationally-derived diagnostics of transport in the lowermost stratosphere and their application to the GMI chemistry transport model, *Atmos. Chem. Phys.*, *7*, 2435–2445.

Strahan, S. E., et al. (2011), Using transport diagnostics to understand chemistry climate model ozone simulations, *J. Geophys. Res.*, *116*, D17302, doi:10.1029/2010JD015360.

Sudo, K., M. Takahashi (2001), Simulation of tropospheric ozone changes during 1997–1998 El Niño: Meteorological impact on tropospheric photochemistry, *Geophys. Res. Lett.*, *28*, 4091–4094.

Tiao, G., G. Reinsel, D. Xu, J. Pedrick, X. Zhu, A. Miller, J. DeLuisi, C. Mateer, and D. Wuebbles (1990), Effects of autocorrelation and temporal sampling schemes on estimates of trend and spatial correlation, *J. Geophys. Res.*, *95*(D12), 20,507–20,517, doi:10.1029/JD095iD12p20507.

Voulgarakis, A., P. Hadjinicolaou, and J. A. Pyle (2011), Increases in global tropospheric ozone following an El Niño event: Examining stratospheric ozone variability as a potential driver, *Atmos Sci Let.*, *12*, doi: 10.1002/asl.318.

Wallace, J. M., R. L. Panetta, and J. Estberg (1993), Representation of the equatorial stratospheric quasi-biennial oscillation in EOF phase space, *J. Atmos. Sci.*, *50*, 1751–1762.

Zeng, G., and J. A. Pyle (2005), Influence of El Niño Southern Oscillation on stratosphere/troposphere exchange and the global tropospheric

ozone budget, *Geophys. Res. Lett.*, *32*, L0814, doi:10.1020/2004GL021353.

Ziemke, J. R., and S. Chandra (1999), Seasonal and inter-annual variabilities in tropical tropospheric ozone, *J. Geophys. Res.*, *104*, 21,425–21,442.

Ziemke, J. R., and S. Chandra (2003), La Nina and El Niño-induced variabilities of ozone in the tropical lower atmosphere during 1970–2001, *Geophys. Res. Lett.*, *30*, 1142, doi:10.1029/2002GL016387.

Ziemke, J. R., S. Chandra, L. D. Oman, and P. K. Bhartia (2010), A new ENSO index derived from satellite measurements of column ozone, *Atm. Chem. Phys.*, *10*, 3711–3721.

Ziemke, J. R., and S. Chandra (2012), Development of a climate record of tropospheric and stratospheric ozone from satellite remote sensing: Evidence of an early recovery of global stratospheric ozone, *Atmos. Chem. Phys.*, *12*, 5737–5753, doi:10.5194/acp-12-5737-2012.